Carbon Trends 17 (2024) 100428

Contents lists available at ScienceDirect

Carbon Trends

journal homepage: www.elsevier.com/locate/cartre

Fe-based catalytic modification of a birch sawdust-based carbon structure: The effect of process parameters on the final product using an experimental design

Henna Lempiäinen [a,b], Davide Bergna [a,b], Anne Heponiemi [a], Tao Hu [a], Glaydson S. dos Reis [c,d], Rafal Sliz [e], Ulla Lassi [a,b,*]

[a] University of Oulu, Research Unit of Sustainable Chemistry, P.O. Box 8000, FI-90014 Oulu, Finland
[b] University of Jyvaskyla, Kokkola University Consortium Chydenius, P.O. Box 567, FI-67100 Kokkola, Finland
[c] Laboratory of Industrial Chemistry and Reaction Engineering, Faculty of Science and Engineering, Åbo Akademi University, 20500 Åbo/Turku, Finland
[d] Biomass Technology Centre, Department of Forest Biomaterials and Technology, Swedish University of Agricultural Sciences, SE-90183 Umeå, Sweden
[e] Research unit of Optoelectronics and Measurement Techniques, P.O. Box 8000, FI-90014 Oulu, Finland

ARTICLE INFO

Keywords:
Birch
Graphite-like structure
Pyrolysis
Conductivity
Iron catalyst
Biomass-based carbon

ABSTRACT

Biomass waste-based, graphite-like material is an interesting alternative to fossil carbons in, for example, battery solutions. The aim was to produce carbon with a graphite-like structure from birch waste through catalytic modification with iron nitrate at relatively low temperatures. The study highlighted the effects of the Fe/birch mass ratio (0–20 mg Fe/g birch), heating temperature (750–900 °C), holding time (1–6 h), and heating rate (3–10 °C/min) on the carbon. The influence of each factor was demonstrated using a design of experiments (DoE) approach. Changes in yield, chemical composition, morphology, specific surface area, total pore volume, pore size distribution, particle size, tapped density, and conductivity were analyzed. The results showed that temperature affected the chemical content, yield, and conductivity. Iron-impregnation affected the structure of birch by modifying its total pore volume, tapped density, I_D/I_G value, and conductivity. The heating rate and holding time had relatively little effect. The highest conductivity (7.23 S/cm) was obtained when impregnated birch was pyrolyzed at the maximum temperature, holding time, and heating rate. However, the best graphitization result (I_D/I_G 0.98) was obtained when iron-impregnated birch was heated for 6 h at 750 °C at a heating rate of 3 °C/min.

1. Introduction

Graphite has become particularly important in recent years for many applications, such as spintronics, heat refractories, lubricants, electrodes, and lithium-ion (Li-ion) batteries [1–6]. It has a multilayered crystalline carbon structure and excellent electrical conductivity, high thermal stability, and chemical stability [7–9].

The European Union has classified graphite as a strategic, critical mineral [10]. It can occur naturally or be prepared synthetically. Typically, synthetic graphite is produced through chemical vapor deposition [11] or thermal graphitization at relatively high temperatures of 1800–3500 °C, usually from coal tar pitch or petroleum coke precursors [12–14]. The conversion of amorphous carbon into high-crystalline graphite can require weeks of processing [15], which is energy intensive, requires specific reactor materials, generates high carbon emissions and environmental pollution, and consumes raw materials unsustainably [16,17]. The development of a graphite production process and graphite anodes that can overcome these problems and produce graphite appropriate for Li-ion batteries has attracted considerable interest [18].

In recent years, biomass has been researched as a renewable, sustainable, and reasonably carbon-neutral source of carbon for graphite production [19,20]. However, biomass is heterogeneous, which poses challenges for the graphitization process. Its poor electrical and thermal conductivity and instability are also challenging for its utilization [21]. Nevertheless, there have been promising results regarding the graphitization of biomass. Kraft black liquor has been successfully graphitized at 2000 °C [22]. Carbon from hydrolysis lignin also exhibited good

* Corresponding author.
E-mail address: ulla.lassi@oulu.fi (U. Lassi).

https://doi.org/10.1016/j.cartre.2024.100428
Received 2 August 2024; Received in revised form 6 November 2024; Accepted 12 November 2024
Available online 17 November 2024

electrochemical performance [23], and cellulose fibers were graphitized to graphite with high electrical conductivity and mechanical properties by laser graphitization [24]. High process temperatures inevitably cause high energy consumption and pollution and require specific equipment. Graphite prepared from biomass may have desirable properties, such as good specific surface area (SSA), pore size distribution, and conductivity [25,26], but tuning graphite-like structures, controlling porosity, and tailoring raw biomass [27] can be difficult.

To meet these challenges, researchers have considered the transition metal-based catalytic graphitization of biomass [28–33]. The process temperatures required for catalytic graphitization can be relatively low (under 1400 °C), which reduces equipment requirements and energy demand [29–31]. Thompson et al. [27] reported obtaining graphitic carbon via iron-catalyzed graphitization of softwood at 800 °C, and Xia et al. [32] obtained mesoporous graphitic carbon at 700–800 °C. Hoekstra et al. [30] showed that iron salt promoted the graphitization of cellulose at 700–800 °C. Sun et al. [33] used iron nitrate to graphitize pine dust and found that the graphite structure formed at 700 °C.

It is known that the properties of the products depend heavily on factors such as the precursors and chemicals used and the conditions under which they are made [34], and it is extremely difficult to understand which of these factors affect the properties of the prepared materials and how they do so; for instance, the graphitization process is largely influenced by the type of catalysts used and their quantities, as well as the pyrolysis conditions (temperature, holding time, and heating rate). To tackle this issue, the design of experiments (DoE) is widely used to study the preparation of materials when several variables influence a process [34]. The DoE methodology makes it possible to identify, rapidly and easily, which significant factors affect the desired material properties, such as the degree of graphitization and conductivity of biomass-based materials, and how they do so.

Woody biomass, such as birch sawdust, is an abundant renewable source of carbon that cannot be used for food production [35–38]. In Finland, 2.9 million m^3 of sawdust and 10.9 million m^3 of solid forest industry by-products were used for energy generation in 2022 [39]. Therefore, in this paper, the authors propose employing birch waste as a low-cost and sustainable precursor for producing graphite-like carbon materials. The research aim was to understand how process parameters affect birch-based carbon materials and especially on their conductivity and graphitization degree. The researchers impregnated biomass with $Fe(NO_3)_3$ at different concentrations, and then conducted slow pyrolysis at a heating rate of 3–10 °C/min. The effects were researched using a DoE approach. The properties of the products were analyzed using various methods, such as Raman spectroscopy, x-ray diffraction (XRD), x-ray photoelectron spectroscopy (XPS), and inductively coupled plasma optical emission spectroscopy (ICP-OES), to analyze the effects of process parameters on yield, chemical composition, morphology, SSA, total pore volume, pore size distribution, particle size, tapped density, and conductivity, and the correlations among these factors were analyzed using principal component analysis (PCA).

2. Experimental

Birch sawdust was collected from a papermill of Metsä Board in Husum in 2016. Sawdust was homogenized using a Fritsch Pulverisette 19 cutting mill with a 0.5-mm sieve.

The sawdust batch was then washed with 0.1 M of nitric acid (nitric acid pro analysis, 65 % Merck KGaB) for 3 h at 50 °C to remove coarse impurities. The mixture was filtrated and rinsed with water until it reached a pH of 7. The washed sawdust was finally dried at 105 °C for 24 h.

The sample was impregnated with an iron catalyst by preparing a mixture of iron nitrate (iron(III) nitrate VWR AnalaR Normapur® analytical reagent) and water and mixing the liquid with sawdust for 2 h at 50 °C. The mixture was dried at 120 °C until all the water evaporated from the sample. Impregnation was applied to mass ratios of 10 and 20 mg Fe/g sawdust.

The experiments were designed using the DoE method. A two-level factorial design was applied to screen for the factors that affected the formation of a graphite-like structure. The graphitization experiment was designed with Origin 2018 software (OriginLab® Corporation, Massachusetts, USA) using four initial factor parameters: Fe and birch mass ratio, heating temperature, holding time, and heating rate. The sequence of randomized values for each trial is presented in Table 1.

The experiments were performed in ceramic vessels placed in a steel reactor in horizontal position. 125 cm3 sample was weighted and then heated in a Nabertherm RT 50/250/13-P320 tubular oven under constant 9.9 mln/min nitrogen flow. The oven's digital controller was programmed according to the DoE matrix before each run. To remove the Fe catalyst and the resulting impurities the sample was finally washed with 3 M nitric acid at 85 °C for 3 h. A reflux column was set up to minimize the loss of liquid. Then the sample was filtrated and rinsed with distilled water until the pH reached 7. The washed sample was then dried at 120 °C.

2.1. Yield

The mass of the sample was weighted before and after pyrolysis, and the yield was calculated as follows:

yield = mass of product (dry basis) / mass of feed (dry basis)* 100%(1)

2.2. SSA, total pore volume, pore size distribution, and particle size distribution

SSA and total pore volume were determined using adsorption–desorption isotherms. The Micromeritics ASAP™ 2020 (Norcross, Georgia, USA) gas adsorption instrument was used with nitrogen as the adsorbate. Before determining isotherms, samples were degassed at 2.7 mbar pressure at 140 °C for 3 h to remove adsorbed gases from the pores and clean the surfaces. Isotherms were determined by placing degassed tubes in liquid nitrogen to achieve isothermal conditions and small doses of nitrogen were then added to obtain adsorption isotherms. SSA values were calculated using the Brunauer–Emmet–Teller (BET) method [40], and total pore volume and pore size distribution were determined according to the non-local density functional theory (NLDFT) [41], assuming the slit geometry of pores. Particle size distribution was determined using a MALVERN Mastersizer 3000 particle size analyzer (Malvern, UK), which bases calculations on static light scattering and Mie theory.

2.3. Tapped density

Tapped density was determined with an Erweka SVM222 density volumenometer (Erweka GmbH, Germany). For determination, the sample was tapped 750 times at a height of 3 mm. The tapped density was calculated as follows:

tapped density = mass of sample / volume of sample after tapping (2)

2.4. XPS

XPS analyses were performed using an ESCALAB™ 250Xi XPS system (Thermo Fisher Scientific, Waltham, USA). The carbon samples were placed on an Au sample holder. The monochromatic AlKα radiation (1486.7 eV) was operated at 20 mA and 15 kV, with a pass energy of 20 eV and a spot size of 900 μm. O and C elemental data were collected for all samples. The measured data were analyzed using Avantage V5 software. Charge compensation was used to calibrate the binding energy

(BE) by applying the C1s line at 284.8 eV as a reference.

2.5. Elemental analysis and field emission scanning electron microscopy (FE-SEM)

Elemental analysis was performed using a Flash™ 2000 CHNS-O organic elemental analyzer (Thermo Scientific, Waltham, USA). The ground sample was first weighed at 1.5–3.5 mg and dried for 1 h at 105 °C. The sample was then placed in the analyzer and mixed with 10 mg of vanadium pentoxide V_2O_5 to enhance burning. The prepared sample was then combusted at a temperature of 960 °C for 600 s using a standard methionine for hydrogen and nitrogen but the BBOT 2,5-(Bis (5-tert-butyl-2-benzo-axazol-2-yl) thiophene standard for oxygen.

FE-SEM was used to study the microstructure of the samples, and FE-SEM images were obtained using a Zeiss Sigma field emission scanning electron microscope (Carl Zeiss Microscopy GmbH, Germany) operated at 5 kV.

2.6. ICP-OES

For the ICP-OES measurements, an Agilent 5110 SVDV (Agilent Technologies Inc., California, USA) instrument was used to compare the total metal content (ashes). Samples weighing 0.3 g were first digested with 9 mL of HNO_3, 2 mL of HCl, and 2 mL of HF at 150 °C for 10 min in a microwave oven (Milestone ETHOS UP, Milestone Inc., Italy). The temperature was then increased to 180 °C in 10 min and after reaching desired temperature, it was maintained for 10 min. Thereafter, the solution was diluted to 50 mL with water, and the elements were analyzed using the ICP-OES method. The results are reported as mg of ashes/g of the sample.

2.7. XRD analysis

An X'pert Pro X-ray diffractometer (Malvern Panalytical, The Netherlands) with monochromatic CuKα1 radiation ($\lambda = 1.5406$ Å) at 45 kV and 40 mA was used to analyze the carbon phase composition. The diffractograms were collected in the 2Θ range of 6–90° at 0.017 intervals with a scan step time of 90 s. The raw data were analyzed using HighScore Plus software.

2.8. Raman spectroscopy

The Raman spectra of the materials were obtained using a time-resolved PicoRaman spectrometer (Timegate Instruments Ltd., Finland). The measurements were conducted at a wave number range of 100–2100 cm^{-1} with ~5 cm^{-1} spectral resolution, and the samples were rotated during the measurements. The PicoRaman instrument uses a 532-nm pulsed laser with a shot length of 150 ps and a frequency of 40–100 kHz.

The Raman spectral data were normalized using the Origin software (OriginLab Corporation, Massachusetts, USA), and Lorentz fitting was used to fit the G and D bands. The integrated areas of the fitted peaks were used to calculate the I_D/I_G ratios of the materials.

2.9. Conductivity measurements

The conductivity of the samples was measured using an 8 mm diameter sample holder, with the sample material positioned between two conductive electrodes. Measurements were taken at intervals of 200 kg/cm^2. For each interval, a stabilization time of 1 min was allowed, followed by three separate readings. The pressure was monitored using a Flintec pressure gauge (Flintec, USA) situated at the base of the holder. Subsequently, the average of the three readings was calculated and presented in the plots.

2.10. Energy-filtered transmission electron analysis

The morphology and microstructure of the carbon materials were also studied using an energy-filtered transmission electron microscope (EF-TEM) with scanning transmission electron microscopy (STEM; JEOL JEM-2200FS EFTEM/STEM [JEOL Ltd. 3–1–2 Musashino, Japan]). The samples were dispersed in ethanol and pretreated in an ultrasonic bath for several minutes. A small drop of the microemulsion was deposited on a copper grid precoated with carbon (Lacey C) and then evaporated in air at room temperature. The accelerating voltage and emission current for the measurements were 120 kV and 8–15 μA, respectively.

2.11. Primary component analysis

PCA was applied to the data using Origin 2018 software (OriginLab Corporation, Massachusetts, USA).

3. Results and discussion

The formation of a graphite-like structure was researched by processing biomass at relatively low temperatures. The experimental setup of the research is described in Table 1. The parameters, mass Fe/birch ratio (0–20 mg Fe /g birch), heating temperature (750–900 °C), holding time (1–6 h), and heating rate (3–10 °C/min) were chosen according to a literature review and the limitations of the oven.

According to the elemental analysis (Table 2), the birch sawdust was mainly composed of carbon (47.1 wt%) and oxygen (45.0 wt%), which are the main components of cellulose and hemicelluloses [42]. The large amounts of C and O made the chosen biomass suitable for carbon material preparation. The birch also contained some natural Fe (0.028 mg/g).

The birch sawdust turned from light brown to black during pyrolysis. According to the FE-SEM and EF-TEM images (Fig. 1), the most important changes were the sharper edges of the particles and rougher surfaces after the experiment. Particle sizes decreased from Dx90 973 μm, Dx50 431 μm, and Dx10 71.6 μm to Dx90 294–819 μm, Dx50 174–356 μm, and Dx10 59.8–105 μm. This decrease in particle size can be explained by the reduction of mass during pyrolysis. It has been reported that water, carbon dioxide, and carbon monoxide evaporate below 300 °C [43]. If the temperature continues to increase, low molecular weight gaseous and volatile products form [44]. Thus, operating conditions, such as temperature and heating rate, affect particle sizes and yields. For example, at low temperatures or low heating rates, char yields are

Table 1
Design of experimental matrix for the experimental setup.

Sample name	Trial	Mass ratio, mg Fe/g birch	Heating rate, °C/min	Temperature, °C	Holding time, h
C1	1	10	6.5	825	3.5
C2	2	20	10	750	6
C3	3	0	10	750	1
C4	4	0	3	900	6
C5	5	20	3	900	1
C6	6	0	3	750	1
C7	7	0	3	750	6
C8	8	20	10	750	1
C9	9	0	10	900	1
C10	10	10	6.5	825	3.5
C11	11	0	3	900	1
C12	12	20	3	900	6
C13	13	0	10	900	6
C14	14	20	3	750	1
C15	15	20	3	750	6
C16	16	20	10	900	1
C17	17	0	10	750	6
C18	18	20	10	900	6
C19	19	10	6.5	825	3.5

Table 2
Elemental analysis (C, O, H, S, N) and main trace inorganic elements (according to ICP-OES) of birch sawdust.

Element	wt%	Element	mg/g
C	47.1	Ca	0.642
O	45.0	Cu	< 0.006
H	6.1	Fe	0.028
S	0.0	K	0.497
N	0.0	Mg	0.178
		Na	0.019
		Ni	< 0.004
		P	0.113
		Zn	0.022

higher [45,46].

The composition analysis (Table 3) highlight that the preparation conditions affected the C content. All the products exhibited a high C content of 71.4–87.1 wt%. For comparison, commercial activated carbon has 88 % C content [47], while commercial graphite has over 98–99 % C content. Correa et al. [47] pyrolyzed different biomass materials, including xylan, alpha-cellulose, and kraft lignin, to produce activated carbons, and their C content varied between 76.9 and 87.8 wt%. Our results showed that the prepared carbon material had a relatively high C content, which is desirable in bio-based materials due to the heightened physicochemical and electrical properties of the carbon. In addition, a high C content can indicate lower ash content, which is beneficial for energy storage applications.

Samples treated at higher temperatures contained more carbon, but the yields and N, H, and O content decreased. This indicated that more volatile gases and tar were released when treatment was performed at a higher (900 °C) rather than a lower (750 °C) temperature. The yield was 28.0–32.2%, whereas the C content of birch was 47.1 wt%, showing that some carbon was lost during pyrolysis. A longer holding time and a higher mass ratio decreased both the H and O content. A faster heating rate promotes the accelerated cracking of organic components and volatile products [48], which leads to decreased yields. After 6 h of holding time, more volatile gases were released than after 1 h, but a longer holding time reduced the yield. This was also visually noticed during the process. After 1 h, some gas was still released from the process, but after 6 h, no visually detected gases were released.

XPS analysis was conducted to evaluate the effect of four process parameters on the surface element composition, chemical state, and functional groups. The carbon spectra (C1s) of the samples were deconvoluted as six peaks (from Scan A to Scan F) related to graphite, aliphatic, C–OH, C = O, O–C = O, and π–π* bonds, respectively. However, the carbon spectra of birch had four peaks: C–C, C–OH, C = O, and O–C = O. Whereas the percentage of C–OH bonds in the samples was lower than the percentage of birch, the percentage of O–C = O bonds remained steady even after the process ended. The oxygen spectra (O1s) of the other samples were deconvoluted into five peaks (C = O, C–OH, C–O, O–C = O, and H_2O bonds), while the O1s spectra of birch were fitted to four peaks (C = O, C–O, C–OH, and O–C = O bonds). The nitrogen spectra (N1s) of birch had a C–N peak, which was also present in the spectra of the treated samples, but after the process, a nitrate peak was also observed that resulted from the nitrate acid wash.

SSA is a very important feature of bio-based materials that has a massive impact on environmental and energy applications [49]. The highest SSA (Table 4) was gained with a 3 °C/min heating rate, with 6 h of heating at 750 °C without a catalyst (C7), highlighting that the methodology employed in this work generated some materials with very well-developed porosity. It has been reported that a high surface area

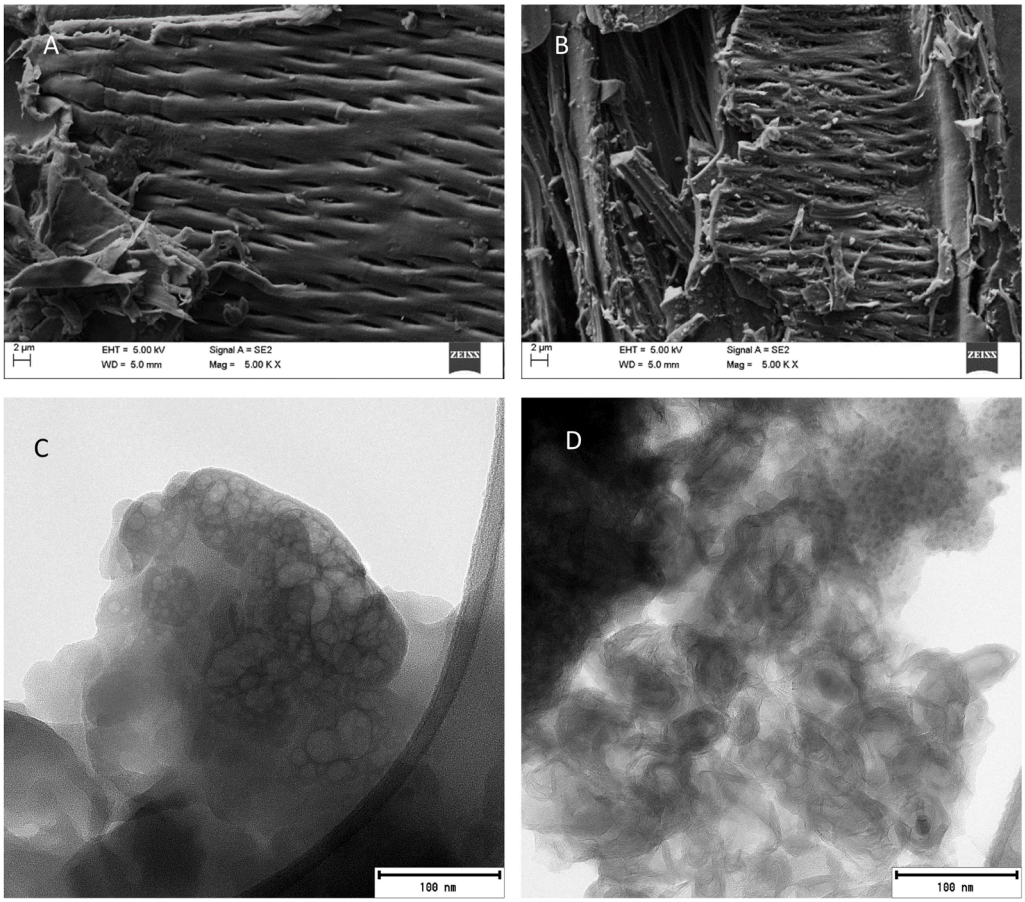

Fig. 1. FE-SEM images of birch sawdust before (A) and after (B) heat treatment (trial 3) and EF-TEM images of C3 (C) and C15 (D).

Table 3
C, N, H, and O content of samples treated according to the DoE setup for birch sawdust before treatment and the yields.

Sample	C, wt%	N, wt%	H, wt%	O, wt%	Yield,%
Birch	47.1	0.0	6.1	45.0	–
C1	81.6	1.5	1.3	8.5	29.8
C2	73.9	1.9	1.6	11.6	29.8
C3	75.3	2.2	2.1	14.6	30.8
C4	84.2	1.3	1.2	9.7	28.6
C5	84.7	1.3	1.0	7.2	29.8
C6	81.5	2.1	2.0	14.3	31.3
C7	76.5	1.8	1.6	13.3	30.5
C8	75.5	2.5	2.0	15.6	30.3
C9	71.6	1.8	1.7	10.9	29.0
C10	81.0	1.1	1.3	9.0	28.8
C11	87.1	1.5	1.4	10.2	29.6
C12	83.8	1.1	0.9	6.3	30.3
C13	84.1	1.2	1.2	8.5	28.0
C14	82.9	2.2	2.0	15.3	32.2
C15	71.4	1.6	1.3	10.7	30.8
C16	79.3	1.2	0.9	8.3	28.6
C17	84.4	1.9	1.8	12.9	29.0
C18	79.6	1.0	0.7	7.7	29.3
C19	85.7	1.5	1.3	9.4	29.4

and the presence of micro/mesopores improve the mass transfer of Li^+ ions in porous carbon anodes [50,51]. Catalyst impregnation increased the total pore volume of the samples. The highest total pore volume (0.20 cm^3/g) resulted from a 3 °C/min heating rate, 6 h of heating at 900 °C, and catalyst impregnation (C12). The pore sizes of the treated samples were mainly smaller than the pore sizes of the birch, except for C8, C9, C11, and C13.

The tapped density of birch was 0.28 g/cm^3. The processed samples were lighter, varying from 0.21 to 0.26 g/cm^3. It has been reported that density affects the electrical conductivity of natural graphite [52]. Increasing the density of graphite from 1.95 g/cm^3 to 2.03 g/cm^3 increased the conductivity from 12.4 S/m with 1 S/m. In our experiment, the variation in tapped density was slight. However, Cai and Fan [53] reported that porosity and high contact resistance caused lower conductivity in mesocarbon microbeads, even though the tap density (1.420 g/cm^3) was higher than the tap density of needle coke (0.902 g/cm^3). In our experiments, both Fe content and tapped density clearly correlated with Fe impregnation because there was more Fe and Fe was denser than carbon.

The conductivity of the samples was measured, as was the conductivity of a commercial graphite as a reference sample. The conductivity of commercial graphite reached values greater than 40 S/cm. The conductivity of the treated birch remained below 2.5 S/cm (Fig. 2). The four highest conductivity values (C5 4.0 S/cm, C12 4.0 S/cm, C16 2.7 S/cm, and C18 7.2 S/cm at 3000 kg/cm^2) were achieved with samples impregnated with Fe and heated to 900 °C with 1 h or 6 h of holding time. Impregnation with Fe affected the conductivity of the samples, with not only graphite but also Fe having higher conductivity than wood. According to Table 4, some Fe impregnated into the samples remained therein after the second acid wash. A high percentage of mesopores and a high surface area are reportedly beneficial for batteries due to Li^+ intercalation [51]. Sample C7 had the highest SSA (390 m^2/g), but low conductivity (0.0 S/cm). These results show the importance of a balance between conductivity and porosity in producing defective sites. Of all pores, 95 % were micropores, which is not beneficial for mass transfer. The four samples with the highest conductivity had SSAs of 135–191 m^2/g and percentages of mesopores and micropores of 63–69 % and 24–36 %, respectively.

Raman spectroscopy was used to analyze amorphous, crystalline, and non-crystalline carbon materials (Supplementary material). Low I_D/I_G values indicate a high degree of graphitization. The I_D/I_G values varied from 0.98 to 5.94, but the Lorentz curve did not fit the spectra for C11–C13 as well as for other samples. Higher temperatures reduced the mean I_D/I_G value, indicating that the proportion of the graphite-like carbon structure increased, and the proportion of the disordered structure decreased. C15 had the lowest I_D/I_G value and the highest degree of graphitization. The result is interesting while it had low conductivity (0.25 S/cm) at 3000 kg/cm^2 whereas C18 had the highest conductivity (7.2 S/cm) but an I_D/I_G value of 2.36. Hard and soft carbon can also have good electrochemical properties [54,55]. They have graphene phases that are not as structured as graphite and its amorphous nonconductive regions do not disturb its electrochemical properties. This may also explain the conductivity of C18.

Fig. 3 shows the XRD patterns for the C3, C5, C10, and C18, which had different graphitic structures. A sharp peak at 2θ 24° was observed in the C5, C10, and C18. The peak at 2θ 24° is associated with the C (002) plane [56], which could be attributed to the packed graphene layers, but could also relate to graphite crystallites. The small peak at 2θ

Table 4
Results for treated samples and birch sawdust.

Sample	SSA, m^2/g	Micropore (< 2 nm), %	Mesopore (2–50 nm), %	Macropore (> 50 nm), %	Total pore volume, cm^3/g	Fe content, mg/g	Tapped density, g/cm3	I_D/I_G, -
Birch	*	36	48	16	0.00	0.03	0.28	–
C1	152	44	55	0	0.11	0.42	0.26	4.27
C2	103	39	60	0	0.08	0.72	0.25	3.80
C3	*	100	0	0	0.00	0.06	0.23	4.83
C4	54	92	7	1	0.02	0.10	0.24	3.61
C5	135	31	69	0	0.12	0.66	0.24	3.90
C6	*	100	0	0	0.00	0.05	0.23	3.50
C7	390	95	5	0	0.14	0.07	0.21	5.69
C8	68	27	58	15	0.08	0.83	0.25	3.37
C9	*	0	75	25	0.01	0.58	0.24	5.94
C10	178	35	61	4	0.15	1.00	0.24	4.04
C11	24	21	59	19	0.03	0.09	0.25	7.86**
C12	160	24	68	8	0.20	0.47	0.25	7.03**
C13	4	0	78	22	0.03	0.05	0.26	4.73**
C14	29	48	50	2	0.02	0.78	0.25	3.71
C15	106	40	59	0	0.08	0.76	0.25	0.98
C16	166	36	63	1	0.14	0.77	0.26	2.70
C17	2	0	99	1	0.00	0.05	0.25	3.45
C18	191	33	66	1	0.16	1.00	0.25	2.36
C19	129	38	61	1	0.10	1.16	0.23	3.03

- Not analyzed.
* No applicable data points.
** Fitting not ideal.

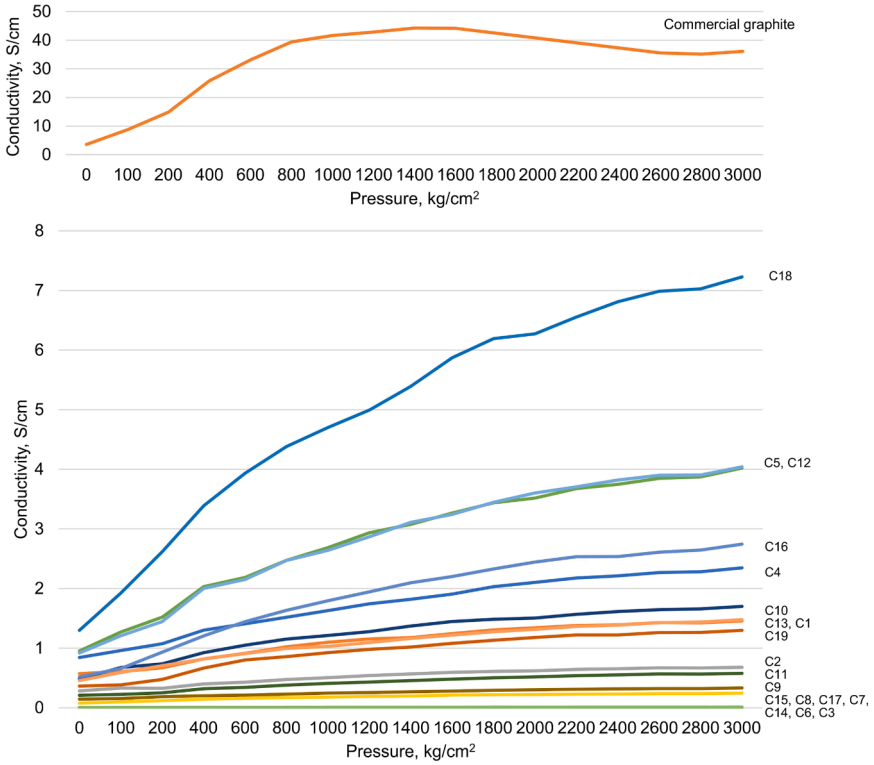

Fig. 2. Conductivity of samples and commercial graphite.

43°, which almost disappeared in the C3, was associated with C (100) diffraction of graphitic carbons, indicating a certain degree of aromatization in the carbon structures. It seems that C3 had a much more amorphous structure than others. Well-developed (002) and (100) patterns are beneficial for boosting the electrical conductivity of carbon materials. These peaks were higher in C18, which was prepared at 900 °C with Fe impregnation. The creation of graphitic structures appeared to be maximized at higher temperatures with larger amounts of Fe.

XRD data revealed that structures with similar graphite-like structures formed: hexagonal 2 H (International Center for Diffraction Data [ICDD] PDF 00–041–1487, 04–007–8496, 04–020–4354, 04–016–0554, and 04–016–4291) and rhombohedral 3R (ICDD PDF 01–073–5918, 04–019–9068, and 01–073–5918). A hexagonal graphite-like structure was detected in C1, C5, C8, C10, C12, C15, C16, and C18, whereas a rhombohedral graphite-like structure was detected in C2, C5, C6, C9, and C19. After some treatment procedures (C3, C4, C7, C11, C13, C14,

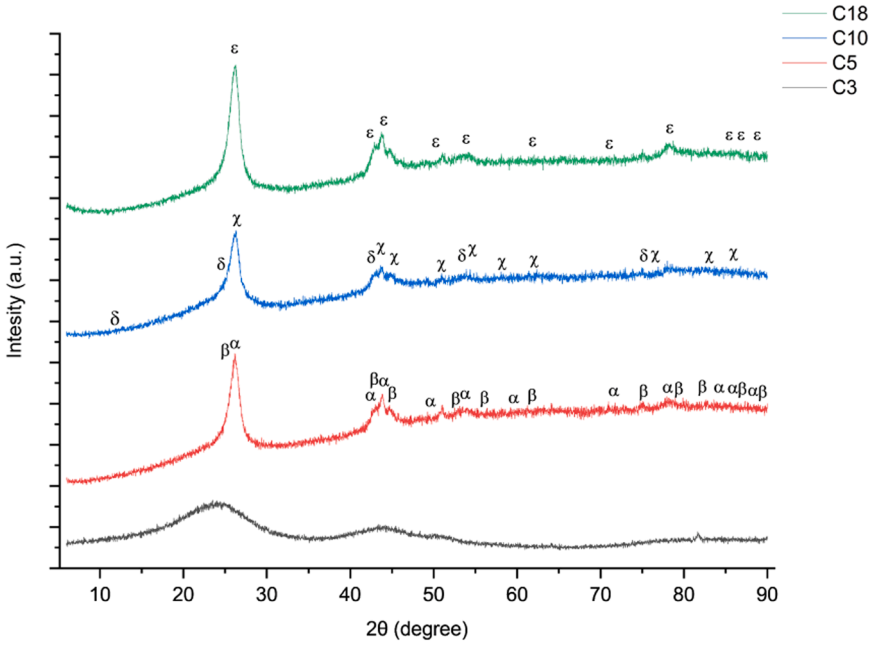

Fig. 3. XRD patterns for samples C5 (hexagonal, α, and rhombohedral graphite, β), C10 (carbon nanotubes, δ, and hexagonal graphite, χ), and C18 (hexagonal graphite, ε), which contained graphite-like structures, and C3, which had no graphite-like structure.

and C17), no graphite-like structures were detected. These samples were treated without Fe impregnation, except for C14. Sample C14 was treated at a low temperature, low heating rate, and short holding time. The XRD pattern for C10 suggested that carbon nanotubes (ICDD PDF 00–058–1638) formed. Wide peaks in patterns are challenging to read, and the peaks of each graphite structure are difficult to distinguish.

Fig. 4 summarizes the statistically significant standardized effects of the process parameters. The temperature at which pyrolysis was conducted had the greatest effect on conductivity, yield, and H, N, O, and C content. Temperature is known as the most important parameter for graphitization processes; therefore, choosing the right temperature is important for controlling the products' physicochemical properties, including conductivity, yield, and carbon content. Xia et al. [32] reported that temperatures over 800 °C caused a significant decrease in amorphous carbon content. A catalyst is important when the total pore volume, tapped density, I_D/I_G value, or conductivity are tuned by choosing certain process parameters. The degree of graphitization increased when the catalyst was used. The catalyst also enhanced the thermal cracking of hydrogen and oxygen [57], but it had no significant effect on the N or C content. Holding time affected composition and yield. The heating rate had a significant effect only on the yield. The effect of process parameters on SSA, pore size distribution, and particle size distribution remained below a significant level.

A PC1/PC2 loading plot (Fig. 5) revealed that Fe and C content, conductivity, total pore volume, and SSA correlated with each other. Fe content and conductivity also correlated strongly with each other. During pyrolysis, O, N, and H were released, which increased the C content and total pore volume and thus led to a higher SSA. The release of volatile and other compounds depends on the temperature [43–46] and holding time. A loss of material during pyrolysis also leads to smaller particles, a lower yield, and a higher C content. Increased C content leads to higher conductivity, but tapped density has no such correlation.

4. Conclusions

The aim of this study was to produce graphite-like material from birch waste using catalytic pyrolysis. The main goal was to determine how the process parameters affected the product. The following process parameters were studied: Fe/birch ratio (0–20 mg Fe/g birch), heating temperature (750–900 °C), holding time (1–6 h), and heating rate (3–10 °C/min). The properties of birch-based products, such as yield, morphology, composition, SSA, pore distribution, tapped density, and conductivity, were investigated using a DoE approach.

Temperature had the greatest effect on the content of the products: it increased the C content and decreased the H, O, and N content, as well as the yield. Holding time had a similar but milder effect. A long heating duration at a high temperature released more volatile compounds and thus increased the C content. In addition, impregnation with an iron catalyst accelerated the cracking of hydrogen and oxygen and reduced their proportions in the samples.

Biomass-based, graphite-like materials used in the anodes of batteries to replace fossil-based graphite, must have good electrochemical properties. However, the production of this kind of material is difficult. Temperature and an iron catalyst showed the strongest correlations with conductivity. The highest conductivity (7.23 S/cm) was achieved by heating the birch with a catalyst for 6 h at 900 °C, with a heating rate of 10 °C/min. However, the conductivity of birch was still significantly lower than the conductivity of commercial graphite (over 40 S/cm) that was used as a reference.

According to the results, the iron catalyst increased the graphitization of the products. The lowest I_D/I_G value (0.98) was achieved by heating the birch with a catalyst for 6 h at 750 °C, with a heating rate of 3 °C/min. Although this degree of graphitization was the highest, the conductivity remained low. The sample with the highest conductivity had a lower degree of graphitization. This may indicate that the sample with high conductivity was closer to conductive hard or soft carbon than graphite.

The iron catalyst also increased the total pore volume of the samples. The highest total pore volume was 0.20 cm^3/g, which was obtained by heating the birch with a catalyst for 6 h at 900 °C, with a heating rate of 3 °C/min. These process conditions also produced one of the highest conductivities 4.0 S/cm. According to the results, samples with high conductivity also had very similar pore size distributions. The samples had 63–69 % mesopores and 24–36 % micropores. None of the process parameters in this research had a significant effect on pore size distribution, nor did they affect the SSA. The highest surface area was 390 m^2/g, which was gained by heating the birch for 6 h at 750 °C, with a heating rate of 3 °C/min. However, the conductivity of this sample was low. PCA showed that total pore volume, C content, and Fe content correlated with conductivity. These results suggest that by adjusting the temperature and iron impregnation, the electrochemical properties of birch can be improved to obtain the desired material.

The results of this research offer insight into the correlations between catalytic graphitization parameters and the properties of birch-based carbon, indicating which parameters are significant for producing graphite-like carbon for batteries. However, further research is required to achieve a biomass-based material with the same characteristics as graphite.

CRediT authorship contribution statement

Henna Lempiäinen: Writing – review & editing, Writing – original draft, Visualization, Methodology, Investigation, Formal analysis, Conceptualization. **Davide Bergna:** Writing – review & editing, Supervision, Conceptualization. **Anne Heponiemi:** Writing – review & editing, Methodology, Formal analysis. **Tao Hu:** Writing – review & editing, Formal analysis. **Glaydson S. dos Reis:** Writing – review & editing,

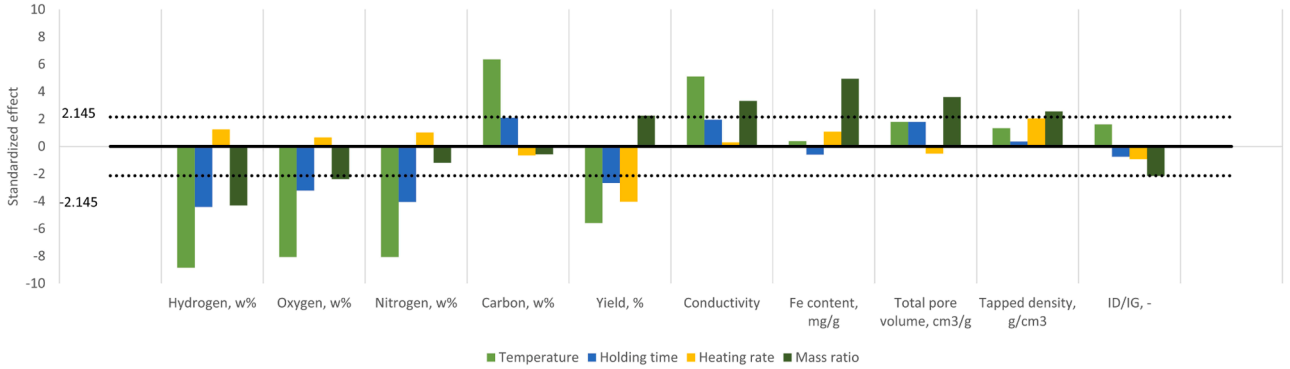

Fig. 4. Standardized effects of process parameters on the product properties (significance lines at 2.145 and −2.145).

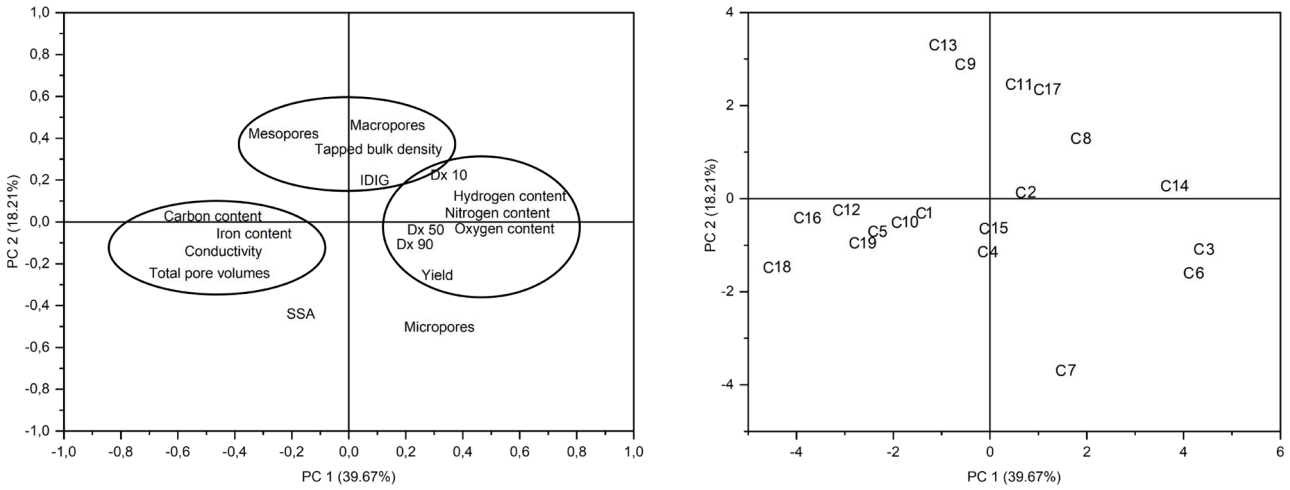

Fig. 5. PC1/PC2 loading plot and score plot for PCA performed on the variables.

Formal analysis. **Rafal Sliz:** Writing – review & editing, Formal analysis. **Ulla Lassi:** Writing – review & editing, Supervision, Project administration.

Declaration of competing interest

The authors declare that they have no known competing financial interests or personal relationships that could have appeared to influence the work reported in this paper.

Acknowledgements

The authors acknowledge the financial support provided by the EU/EURF/Carbotech (A75548), BF/PUMA (4736/31/2019), and EU/InterregAurora/GreenBattery (20357574) projects, and the Central Ostrobothnia Regional Fund (Finnish Cultural Foundation). Dr. Glaydson dos Simoes Reis gratefully acknowledges financial support from the Research Council of Finland (Academy Research Fellows 2024, Project: Bio-Adsorb&Energy, grant no 361583). The authors thank the staff of the Center of Microscopy and Nanotechnology, University of Oulu, for their assistance during the XPS analyses, technical assistants of Sustainable Chemistry, University of Oulu, for elemental and ICP-EOS analyses, and Biomass Technology Centre, Swedish University of Agricultural Sciences, for birch.

Supplementary materials

Supplementary material associated with this article can be found, in the online version, at doi:10.1016/j.cartre.2024.100428.

Data availability

Data will be made available on request.

References

[1] A.D. Jara, A. Betemariam, G. Woldetinsae, J.Y. Kim, Purification, application and current market trend of natural graphite: a review, Int. J. Min. Sci. Technol. 29 (2019) 671–689, https://doi.org/10.1016/j.ijmst.2019.04.003.
[2] F. Alidad, R. Navik, Y. Gai, Y. Zhao, Production of pristine graphene quantum dots from graphite by a shear-mixer in supercritical CO2, Chem. Phys. Lett. 710 (2018) 64–69, https://doi.org/10.1016/j.cplett.2018.08.073.
[3] C. Baudin, C. Alvarez, R.E. Moore, Influence of chemical reactions in magnesia-graphite refractories: I, effects on texture and high-temperature mechanical properties, J. Am. Ceram. Soc. 82 (1999) 3529–3538, https://doi.org/10.1111/j.1151-2916.1999.tb02276.x.
[4] Z. Jian, Z.Y. Piao, S.Y. Liu, S.W. Su, L.J. Deng, Investigation of wear behavior of graphite coating on aluminum piston skirt of automobile engine, Eng. Fail. Anal. 97 (2019) 408–415, https://doi.org/10.1016/j.engfailanal.2019.01.012.
[5] Y.P. Wu, X.Y. Liu, D.D. Xia, Q.S. Sun, D.Y. Yu, S.G. Sun, et al., Synthesis of few-layer N-doped graphene from expandable graphite with melamine and its application in supercapacitors, Chin. Chem. Lett. 31 (2020) 559–564, https://doi.org/10.1016/j.cclet.2019.04.055.
[6] J. Xu, X. Wang, N.Y. Yuan, B.Q. Hu, J.N. Ding, S.H. Ge, Graphite-based lithium ion battery with ultrafast charging and discharging and excellent low temperature performance, J. Power Source. 430 (2019) 74–79, https://doi.org/10.1016/j.jpowsour.2019.05.024.
[7] J. Kim, O. Song, Y.S. Cho, M. Jung, D. Rhee, J. Kang, Revisiting solution-based processing of van der Waals layered materials for electronics, ACS Mater. Au 2 (4) (2022) 382–393, https://doi.org/10.1021/acsmaterialsau.2c00034.
[8] Q. Chen, X.F. Tan, Y.G. Liu, S.B. Liu, M.F. Li, Y.L. Gu, et al., Biomass-derived porous graphitic carbon materials for energy and environmental applications, J. Mater. Chem. 8 (2020) 5773–5811, https://doi.org/10.1039/C9TA11618D.
[9] X. Zhang, B. Sun, X. Fan, P. Liang, G. Zhao, B.K. Saikia, et al., Hierarchical porous carbon derived from coal and biomass for high performance supercapacitors, Fuel 311 (2022), https://doi.org/10.1016/j.fuel.2021.122552. Article 122552.
[10] S. Bobba, S. Carrara, J. Huisman, F. Mathieux, C. Pavel, Critical materials for strategic technologies and sectors in the EU: a foresight study, Publications Office of the European Union, Luxembourg (2020), https://doi.org/10.2873/58081.
[11] Y. Zhang, H. Shu, Z. Chen, G. Mu, Y. Sui, Y. Liang, et al., Chemical vapor deposition growth and characterization of graphite-like film, Res. Expr. 7 (2020) 015609, https://doi.org/10.1088/2053-1591/ab664b.
[12] S. Huang, H. Guo, X. Li, Z. Wang, L. Gan, J. Wang, W. Xiao, Carbonization and graphitization of pitch applied for anode materials of high power lithium ion batteries, J. Solid State Electrochem 17 5 (2013) 1401–1408, https://doi.org/10.1007/s10008-013-2003-9.
[13] B. Xing, C. Zhang, Y. Cao G. Huang, Q. Liu, C. Zhang, et al., Preparation of synthetic graphite from bituminous coal as anode materials for high performance lithium-ion batteries, Fuel Process. Technol. 172 (2018) 162–171, https://doi.org/10.1016/j.fuproc.2017.12.018.
[14] C. Li, B. Xie, D. Chen, J. Chen, W. Li, Z. Chen, et al., Ultrathin graphite sheets stabilized stearic acid as a composite phase change material for thermal energy storage, Energy 166 (2019) 246–255, https://doi.org/10.1016/j.energy.2018.10.082.
[15] L. Gai, J. Li, Q. Wang, R. Tian, K. Li, Evolution of biomass to porous graphite carbon by catalytic graphitization, J. Environ. Chem. Eng. 9 (2021), https://doi.org/10.1016/j.jece.2021.106678. Article 106678.
[16] Y. Yang, J.G. Brammer, D.G. Wright, J.A. Scott, C. Serrano, A.V. Bridgwater, Combined heat and power from the intermediate pyrolysis of biomass materials: performance, economics and environmental impact, Appl. Energy 191 (2017) 639–652, https://doi.org/10.1016/j.apenergy.2017.02.004.
[17] Y. Gao, X. Wang, Y. Chen, P. Li, H. Liu, H. Chen, Pyrolysis of rapeseed stalk: influence of temperature on product characteristics and economic costs, Energy 122 (2017) 482–491, https://doi.org/10.1016/j.energy.2017.01.103.
[18] N.A. Banek, K.R. McKenzie Jr, D.T. Abele, M.J. Wagner, Sustainable conversion of biomass to rationally designed lithium-ion battery graphite, Sci. Rep. 12 (2022) 8080, https://doi.org/10.1038/s41598-022-11853-x.
[19] I. Mian, X. Li, O.D. Dacres, J.J. Wang, B. Wei, Y.M. Jian, et al., Combustion kinetics and mechanism of biomass pellet, Energy 205 (2020) 117909, https://doi.org/10.1016/j.energy.2020.117909.
[20] J. Al Asfar, A. AlShwawra, N. Abu Shaban, M. Alrbai, B.R. Qawasmeh, A. Sakhrieh, et al., Thermodynamic analysis of a biomass-fired lab-scale power plant, Energy 194 (2020) 116843, https://doi.org/10.1016/j.energy.2019.116843.
[21] S. Xia, H. Yang, W. Lu, N. Cai, H. Xiao, X. Chen, et al., Fe–Co based synergistic catalytic graphitization of biomass: influence of the catalyst type and the pyrolytic

temperature, Energy 239 (2022) 122262, https://doi.org/10.1016/j.energy.2021.122262.
[22] J. Köhnke, H. Rennhofer, H. Lichtenegger, A. Mahendran, C. Unterweger, B. Prats-Mateu, et al., Electrically conducting carbon microparticles by direct carbonization of spent wood pulping liquor, ACS Sustain. Chem. Eng. 6 (3) (2018) 3385–3391, https://doi.org/10.1021/acssuschemeng.7b03582.
[23] Y. Xi, D. Yang, X. Qiu, H. Wang, J. Huang, Q. Li, K2CO3 activation enhancing the graphitization of porous lignin carbon derived from enzymatic hydrolysis lignin for high performance lithium-ion storage, Ind. Crop. Prod. 124 (2018) 747–754, https://doi.org/10.1016/j.jallcom.2019.01.039.
[24] F. Morosawa, S. Hayashi, M. Terakawa, Femtosecond laser-induced graphitization of transparent cellulose nanofiber films, ACS Sustain. Chem. Eng. 9 (7) (2021) 2955–2961, https://doi.org/10.1021/acssuschemeng.0c09153.
[25] P. Molaiyan, G.S. Dos Reis, D. Karuppiah, C.M. Subramaniyam, F. García-Alvarado, U. Lassi, Recent progress in biomass-derived carbon materials for Li-ion and Na-ion batteries—a review, Batteries 9 (2) (2023) 116, https://doi.org/10.3390/batteries9020116.
[26] D. Alvira, D. Antorán, J.J. Manyà, Plant-derived hard carbon as anode for sodium-ion batteries: a comprehensive review to guide interdisciplinary research, Chem. Eng. J. 447 (2022) 137468, https://doi.org/10.1016/j.cej.2022.137468.
[27] E. Thompson, A.E. Danks, L. Bourgeois, Z. Schnepp, Iron-catalyzed graphitization of biomass, Green Chem. 17 (2015) 551–556, https://doi.org/10.1039/C4GC01673D.
[28] L. Gai, J. Li, Q. Wang, R. Tian, K. Li, Evolution of biomass to porous graphite carbon by catalytic graphitization, J. Environ. Chem. Eng. 9 (2021) 6, https://doi.org/10.1016/j.jece.2021.106678.
[29] W.J. Liu, K. Tian, Y.R. He, H. Jiang, H.Q. Yu, High-yield harvest of nanofibers/mesoporous carbon composite by pyrolysis of waste biomass and its application for high durability electrochemical energy storage, Environ. Sci. Technol. 48 (23) (2014) 13951–13959, https://doi.org/10.1021/es504184c.
[30] J. Hoekstra, A.M. Beale, F. Soulimani, M. Versluijs-Helder, D. van de Kleut, J. M. Koelewijn, et al., The effect of iron catalyzed graphitization on the textural properties of carbonized cellulose: magnetically separable graphitic carbon bodies for catalysis and remediation, Carbon N.Y. 107 (2016) 248–260, https://doi.org/10.1016/j.carbon.2016.05.065.
[31] D.W. Kim, H.S. Kil, J. Kim, I. Mochida, K. Nakabayashi, C.K. Rhee, et al., Highly graphitized carbon from non-graphitizable raw material and its formation mechanism based on domain theory, Carbon N.Y. 121 (2017) 301–308, https://doi.org/10.1016/j.carbon.2017.05.086.
[32] S. Xia, N. Cai, J. Wu, H. Xiao, J. Hu, X. Chen, et al., Synthesis and formation mechanism of biomass-based mesoporous graphitic carbon, Fuel Proc. Technol. 209 (2020) 106543, https://doi.org/10.1016/j.fuproc.2020.106543.
[33] Z. Sun, D. Yao, C. Cao, Z. Zhang, L. Zhang, H. Zhu, et al., Preparation and formation mechanism of biomass-based graphite carbon catalyzed by iron nitrate under a low-temperature condition, J. Env. Manag. 318 (2022) 115555, https://doi.org/10.1016/j.jenvman.2022.115555.
[34] G.S. dos Reis, S.H. Larsson, M. Mathieu, et al., Application of design of experiments (DoE) for optimised production of micro- and mesoporous Norway spruce bark-activated carbons, Biomass Conv. Bioref. 13 (2023) 10113–10131, https://doi.org/10.1007/s13399-021-01917-9.
[35] A.J. Ragauskas, C.K. Williams, B.H. Davison, G. Britovsek, J. Cairney, C.A. Eckert, et al., The path forward for biofuels and biomaterials, Science 311 (2006) 48–89, https://doi.org/10.1126/science.1114736.
[36] V. Menon, M. Rao, Trends in bioconversion of lignocellulose: biofuels, platform chemicals & biorefinery concept, Prog. Energy Combust. Sci. 38 (2012) 522–550, https://doi.org/10.1016/j.pecs.2012.02.002.
[37] P. Sannigrahi, Y. Pu, A. Ragauskas, Cellulosic biorefineries—Unleashing lignin opportunities, Curr. Opin. Environ. Sustain. 2 (2010) 383–393, https://doi.org/10.1016/j.cosust.2010.09.004.
[38] Y. Pu, M. Kosa, U.C. Kalluri, G.A. Tuskan, A.J. Ragauskas, Challenges of the utilization of wood polymers: how can they be overcome? Appl. Microbiol. Biotechnol. 91 (2011) 1525–1536, https://doi.org/10.1007/s00253-011-3350-z.
[39] T. Niinistö, Wood in energy generation 2022, Natural Resources Institute Finland, Finland, 2023.
[40] S. Brunauer, P.H. Emmett, E. Teller, Adsorption of gases in multimolecular layers, J. Am. Chem. Soc. 60 (1938) 309–319, https://doi.org/10.1021/ja01269a023.
[41] C. Lastoskie, K.E. Gubbins, N. Quirke, Pore size heterogeneity and the carbon slit pore: a density functional theory model, Langmuir 9 (10) (1993) 2693, https://doi.org/10.1021/la00034a032.
[42] H. Lempiäinen, K. Lappalainen, M. Mikola, T. Tuuttila, T. Hu, U. Lassi, Acid-catalyzed mechanocatalytic pretreatment to improve sugar release from birch sawdust: structural and chemical aspects, Catal. Today 397-399 (2022) 550–561, https://doi.org/10.1016/j.cattod.2021.06.015.
[43] W.F. Degroot, W.-P. Pan, M.D. Rahman, G.N. Richards, First chemical events in pyrolysis of wood, J. Analyt. Appl. Pyroly. 13 (3) (1988) 221–231, https://doi.org/10.1016/0165-2370(88)80024-X.
[44] F. Shafizadeh, Introduction to pyrolysis of biomass, J. Analyt. Appl. Pyroly. 3 (4) (1982) 283–305, https://doi.org/10.1016/0165-2370(82)80017-X.
[45] A.V. Bridgwater, Catalysis in thermal biomass conversion, Appl. Cat. A: Gen. 116 (1–2) (1994) 5–47, https://doi.org/10.1016/0926-860X(94)80278-5.
[46] Q. Zheng, D. Zhang, P. Fu, A. Wang, Y. Sun, Z. Li, et al., Insight into the fast pyrolysis of lignin: unraveling the role of volatile evolving and char structural evolution, Chem. Eng. J. 437 (1) (2022) 135316, https://doi.org/10.1016/j.cej.2022.135316.
[47] C.R. Correa, T. Otto, A. Kruse, Influence of the biomass components on the pore formation of activated carbon, Biomass Bioenergy 97 (2017) 53–64, https://doi.org/10.1016/j.biombioe.2016.12.017.
[48] C. Li, J.-I. Hayashi, Y. Sun, L. Zhang, S. Zhang, S. Wang, et al., Impact of heating rates on the evolution of function groups of the biochar from lignin pyrolysis, J. Anal. App. Pyroly. 155 (2021) 105031, https://doi.org/10.1016/j.jaap.2021.105031.
[49] S. Bhat, U.T. Uthappa, T. Sadhasivam, T. Altalhi, S.S. Han, M.D. Kurkuri, Abundant cilantro derived high surface area activated carbon (AC) for superior adsorption performances of cationic/anionic dyes and supercapacitor application, Chem. Eng. J. 459 (2023) 141577, https://doi.org/10.1016/j.cej.2023.141577.
[50] Y. Zhang, L. Chen, Y. Meng, J. Xie, Y. Guo, D. Xiao, Lithium and sodium storage in highly ordered mesoporous nitrogen-doped carbons derived from honey, J. Power Sources 335 (2016) 20–30, https://doi.org/10.1016/j.jpowsour.2016.08.096.
[51] A.F. Leonard, A. Castro-Muniz, F. Suarez-García, N. Job, J.I. Paredes, Understanding the effect of the mesopore volume of ordered mesoporous carbons on their electrochemical behavior as Li-ion battery anodes, Micropor. Mesopor. Mat. 306 (2020) 110417, https://doi.org/10.1016/j.micromeso.2020.110417.
[52] S. Rattanaweeranon, P. Limsuwan, V. Thongpool, V. Piriyawong, P. Asanithi, Influence of bulk graphite density on electrical conductivity, Procedia Eng 32 (2012) 1100–1106, https://doi.org/10.1016/j.proeng.2012.02.061.
[53] Y. Cai, C.-l. Fan, Influences of conductive additives on electrochemical performances of artificial graphite anode with different shapes for lithium ion batteries, Electrochim. Acta 58 (2011) 481–487, https://doi.org/10.1016/j.electacta.2011.09.080.
[54] M. Thompson, Q. Xia, Z. Hua, X.S. Zhao, A review on biomass-derived hard carbon materials for sodium-ion batteries, Mater. Adv. 2 (2021) 5881–5905, https://doi.org/10.1039/D1MA00315A.
[55] J.S. McDonald-Wharry, M. Manley-Harris, K.L. Pickering, Reviewing, combining, and updating the models for the nanostructure of non-graphitizing carbons produced from oxygen-containing precursors, Energy Fuel. 30 (10) (2016) 7811–7826, https://doi.org/10.1021/acs.energyfuels.6b00917.
[56] N. Yoshizawa, K. Maruyama, Y. Yamada, M. Zielinska-Blajet, XRD evaluation of CO2 activation process of coal- and coconut shell-based carbons, Fuel 79 (12) (2000) 1461–1466, https://doi.org/10.1016/S0016-2361(00)00011-9.
[57] Q. Yan, J. Li, X. Zhang, J. Zhang, Z. Cai, Synthetic bio-graphene based nanomaterials through different iron catalysts, Nanomat 8 (10) (2018) 840, https://doi.org/10.3390/nano8100840.